# Comparison of 3D Dense Deformable Registration Methods for Breath-hold Reproducibility Study in Radiotherapy

Vlad Boldea[a], David Sarrut[a,b], and Christian Carrie[b]

[a]LIRIS, Université Lumière Lyon 2, 5 Av. P. Mendès-France, 69676 Bron, France
[b] Radiotherapy Dpt, Centre Léon Bérard, 28 rue Laennec, 69008 Lyon, France

## SUMMARY

**1. Description of purpose** The main challenge for lung cancer radiotherapy is to provide prescribed doses to the tumor while sparing surrounding normal tissues. This is a challenging task because of organs and tumors motions. We are involved in a project consisting in immobilizing the organs and tumors by breath-holding (BH). BH is implemented with Active Breath Control (ABC) device, allowing to automatically hold the patient breath according to a predetermined instant in the breathing cycle. The goal is to study internal lung residual motion between several 3D Computerized Tomography (CT) scans acquired on a same patient, at a same level of the breathing cycle.

**2. Material and methods** The goal of non rigid registration methods is to find points correspondences between two or more different images whose mismatched can not be reduced to a simple affine transformation. In this paper, we compare three regularization approaches (Gaussian, linear elastic and Nagel-Enkelmann) associated with the same "demons" forces, proposed by Thirion. For these three regularization technics we used two different iterative implementation schemes. We based our evaluation on clinical data sets of two patients (6 CT scans for each patient) and on a priori clinical knowledge : one patient presents normal lung behavior while the second has impaired lung behavior due to atelectasis and emphysema which lead to bad BH reproducibility. 3D images are first rigidly aligned. Residual motion, is obtained by subtracting the rigid deformation from the computed vector field by non-rigid registration. Several vector field operators (symmetry and transitivity error, Jacobian and volume dilatation) were used for deformation evaluation. For each vector field operator we computed Student's t-test to show if the methods provide significant differences.

**3. Results** Gaussian regularization leads to faster convergence (about 150 iterations) than linear elastic and Nagel-Enckelmann based regularizations which require a minimum of 800 iterations for patient 1 and even more iterations for patient 2 (with larger deformations). We noticed that the symmetry and transitivity errors for each method are relatively larger for patient 2 compared to patient 1. Deformation fields computed with Nagel-Enckelmann regularization present a larger number of negative Jacobian points than two others methods. We also noticed that a global lung contraction implies a larger percentage of points with negative Jacobian. Dilatation operator gives equivalent results for the three methods.

**4. New work to be presented** We used here clinical data sets of two patients : one with normal lung behavior and the second with bad BH reproducibility due to atelectasis and emphysema. For each, 3D CT scans are acquired in BH at a determined level of the breathing cycle (about 70% of the vital capacity). We compare three regularization approaches (Gaussian, linear elastic and Nagel-Enkelmann) associated with the same "demons" forces, proposed by Thirion. Several vector field operators (symmetry and transitivity error, Jacobian and volume dilatation) were used for deformation evaluation.

**5. Conclusions** Breath holding requires the knowledge of residual motion between two breath-holds. Non-rigid registration allows to estimate such residual motion and vector field information will be used for dose margins delivery studies. In this work, we studied three non-rigid registration schemes (Gaussian, linear elastic and Nagel-Enckelmann based regularizations) and analyzed several operators (transitivity, symmetry, dilatation, Jacobian) to compare resulting vector fields. Data sets from two patients with normal and impaired lung behavior were used. None of operators allows to clearly highlight the superiority of a method, except for convergence rapidity and Jacobian. worse). None of the analysis operators used here considers anatomical structures informations, only evaluate vector fields. Future works will exploit vector field properties together with local anatomical structure correspondences.

**6. Note** We submitted to International Journal of Radiation Oncology Biology Physics a paper with first results of reproducibility study of breath holding with ABC. Only deformable registration with Gaussian regularization was presented. Vector field operators have been only mentioned but not studied as we do here.

# Comparison of 3D Dense Deformable Registration Methods for Breath-hold Reproducibility Study in Radiotherapy

Vlad Boldea[a], David Sarrut[a,b], and Christian Carrie[b]

[a]LIRIS, Université Lumière Lyon 2, 5 Av. P. Mendès-France, 69676 Bron, France
[b] Radiotherapy Dpt, Centre Léon Bérard, 28 rue Laennec, 69008 Lyon, France

## ABSTRACT

Breath holding (BH) allows to immobilize organs during radiotherapy treatment of lung cancer. Deformable registration methods applied on 3D Computerized Tomography (CT) scans acquired in BH can be used to evaluate the breath holding reproducibility. Resulting 3D vector fields could then be used to adapt internal margins for each patient. In this work we compare three non-rigid registration schemes with Gaussian, linear-elastic and Nagel-Enckelmann based regularizations. As we do not dispose of gold standard, we analyze vector fields by several operators (transitivity, symmetry, volume dilatation, Jacobian). Experiments were based on clinical data sets of two patients: one with normal lung behavior and second with lung discrepancies which lead to bad BH reproducibility. Results show that none of operators allows to clearly highlight the superiority of a method, except for convergence rapidity and Jacobian.

**Keywords:** Non-rigid registration, vector field operators, lung, CT scan, radiotherapy

## 1. INTRODUCTION

The main challenge for lung cancer radiotherapy is to provide prescribed doses to the tumor while sparing surrounding normal tissues. This is a challenging task because of organs and tumors motions. Incorporating organ deformation can be achieved with several approaches[1] : adapting internal margins (as defined in ICRU Report 62[2]), synchronizing radiation delivery with breathing (but it requires invasive internal markers or depend on an hypothetical correlation between external and internal movements[3]) or holding patient breath.

We are involved in a project consisting in immobilizing the organs and tumors by breath-holding (BH). BH is implemented with Active Breath Control (ABC) device,[4] allowing to automatically hold the patient breath according to a predetermined instant in the breathing cycle. The goal is to study internal lung residual motion between several 3D Computerized Tomography (CT) scans acquired on a same patient, at a same level of the breathing cycle. In previous work[5] we proposed the use of non-rigid registration method in order to evaluate breath hold reproducibility, quantify residual motion and detect lung functional abnormalities. In this paper, we compare three regularization approaches (Gaussian, linear elastic and Nagel-Enkelmann) associated with the same "demons" forces, proposed by Thirion[6] and we used several vector field operators for deformation evaluation. We based our evaluation on clinical data sets of two patients (6 CT scans for each patient) and on a priori clinical knowledge : one patient presents normal lung behavior while the second has impaired lung behavior due to atelectasis and emphysema which lead to bad BH reproducibility.

## 2. DENSE NON-RIGID REGISTRATION

### 2.1. General framework

The goal of non rigid registration methods is to find points correspondences between two or more different images whose mismatched can not be reduced to a simple affine transformation. Non rigid registration algorithms were used for multiple purposes on monomodal and multimodal images registration. At our knowledge there are a few works for 3D non rigid registration of thorax CT scans.[7,8] Dense non-rigid intensity based registration algorithm can be expressed as a criterion minimization. The criterion is a trade-off between two energies: similarity energy ($E_1$) and regularization energy ($E_2$). The similarity energy $E_1$ quantifies the images alignment quality. The regularization energy $E_2$ constrains the deformation field to have some spacial coherence. Equation 1

summarizes the general formulation. $U$ denotes a deformation field, $\tilde{U}$ denotes the final solution, $\beta$ $(0 \leq \beta \leq 1)$ denotes a tradeoff factor between the two energies.

$$\tilde{U} = \arg\min_{U}(E(U)) \quad ; \quad E(U)) = (1-\beta)E_1(U) + \beta E_2(U) \tag{1}$$

### 2.2. Registration schemes

**"Demons" with Gaussian regularization.** In previous work,[5] we focused on the "demons" algorithm proposed by Thirion and modified by Cachier.[6,9] This algorithm can be summarized as follows: at each iteration step of an iterative procedure a correction field $u_i$ (eq 2) is computed and the new global field $U_i$ is obtained after Gaussian smoothing ($U_i = smooth(U_{i-1}+u_i)$). $I$ and $J$ denote the images, $Id$ denotes the identity matrix, the $\alpha$ $(\alpha > 0)$ parameter introduced by Cachier[9] limits the displacement vector for small gradients: the norm is bounded by $1/(2\alpha)$. $\boldsymbol{x}$ denotes an image point, $i$ the iteration index and $\nabla$ the gradient operator.

$$u_i(\boldsymbol{x}) = \frac{I(\boldsymbol{x}) - J(Id + U_{i-1}(\boldsymbol{x}))}{\| \nabla I \|^2 + \alpha^2 (I(\boldsymbol{x}) - J(Id + U_{i-1}(\boldsymbol{x})))^2} \nabla I \tag{2}$$

Due to a Gaussian regularization of the vector field, this method can be viewed as an elastic-like algorithm[9] or an homogeneous isotropic diffusion. In order to take into account non-homogeneous nature of the thorax, we implemented two others methods using the "demons" forces for estimating points correspondence and different regularization operators of the vector field: linearized elasticity operator[10,11] and Nagel-Enkelmann operator.[12] For these two regularization technics we used a different iterative implementation scheme compared to the Gaussian regularization.

**Linear elastic regularization.** A solution to the minimization equation 1 can be found by solving the equivalent Euler equations[11] : $\nabla E(\tilde{U}) = 0$. We considered the Euler explicit equation 3 for an iterative implementation of the algorithm. $\kappa$ $(\kappa > 0)$ denotes the descent step size.

$$U_i(\boldsymbol{x}) = U_{i-1}(\boldsymbol{x}) + \kappa((1-\beta)\nabla E_1(U_{i-1}(\boldsymbol{x})) + \beta \nabla E_2(U_{i-1}(\boldsymbol{x}))) \tag{3}$$

Cachier[9] demonstrates that the "demons" forces are closed to a second order gradient descent of an SSD criterion under the hypothesis of small correction field. Under this assumption we used the "demons" forces as gradient of the similarity criterion: $\nabla E_1(U_{i-1}(\boldsymbol{x})) = u_i(\boldsymbol{x})$.

Bro-Nielsen[13] shows that Gaussian regularization is related (under some assumptions) to linear elastic filter. Moreover, linear elastic regularization allows to take into account cross-effects while Gaussian smoothing does not.[14] The general form of the linearized elasticity operator is inspired from the equilibrium equation 4 under the hypothesis of small displacements where $\lambda$ and $\mu$ are the Lamé coefficients and $F$ are the applied volume forces. $F = 0$ if deformation is due to surface forces only. $\nabla \cdot U$ denotes the divergence of $U$ and $\triangle$ the Laplacian operator. The gradient of the regularization energy is computed with linearized elasticity operator summarized by the equation 5. Instead of using Lamé coefficients,[11] introduces $\xi$ $(0 < \xi \leq 1)$ to have a diffusion-like method.

$$(\lambda + \mu)\nabla(\nabla \cdot U) + \mu \cdot \triangle U = -F \tag{4}$$

$$\nabla E_2(U_{i-1}(\boldsymbol{x})) = (1-\xi)\nabla(\nabla \cdot U_{i-1}(\boldsymbol{x})) + \xi \triangle U_{i-1}(\boldsymbol{x}) \tag{5}$$

**Nagel-Enckelmann based regularization.** Anisotropic regularization guided by the image gradient was firstly proposed by Nagel-Enkelmann.[12] Such regularization technique takes into account local structures of the image : it smoothes mainly homogeneous structures and preserves vector field discontinuities across structures boundaries. We used same implementation scheme equation 3 like for linear elastic regularization. The derivative of regularization energy is computed as follows:

$$\nabla E_2(U_{i-1}(\boldsymbol{x})) = \begin{pmatrix} div(W\nabla U^1_{i-1}) \\ div(W\nabla U^2_{i-1}) \\ div(W\nabla U^3_{i-1}) \end{pmatrix} \tag{6}$$

*div* denotes the divergence, $U^1_{i-1}, U^2_{i-1}, U^3_{i-1}$ are the components of the 3D vector field and W is a 3x3 symmetric regularized projection matrix calculated from the $I_x, I_y, I_z$ gradient components of the reference image $I$.

$$W = \frac{1}{2(I_x^2 + I_y^2 + I_z^2) + 3\gamma} \cdot \begin{pmatrix} I_y^2 + I_z^2 + \gamma & -I_xI_y & -I_xI_z \\ -I_xI_y & I_x^2 + I_z^2 + \gamma & -I_yI_z \\ -I_xI_z & -I_yI_z & I_x^2 + I_y^2 + \gamma \end{pmatrix} \tag{7}$$

where $\gamma$ is a parameter for region distinction ($\gamma > 0$). We chose $\gamma$ according to gradient norm values range of the reference image scan. This operator has an almost isotropic behavior for homogeneous regions ($|\nabla I|^2 \ll \gamma$) and an anisotropic behavior along the edges ($|\nabla I|^2 \gg \gamma$).

Differential operators were computed by 3D spatial differences scheme.[11]

We thus have three different ways to compute vector fields: the first method $M_1$ is the "demons" algorithm with Gaussian regularization, the second method $M_2$ with linear elastic regularization and the third $M_3$ with anisotropic regularization.

## 3. VECTOR FIELD COMPARISON

3D images are first rigidly aligned. We applied a 3D rigid registration algorithm[15] by privileging rigid bonny structures. Residual motion, denoted by $U^p$ is obtained by subtracting the rigid deformation $R_{XY}$ from the computed vector field by non-rigid registration: $U^p_{XY} = U_{XY} - R_{XY}$.

Here we study four vector field operators : symmetry and transitivity error, Jacobian and volume dilatation. For each vector field operator we computed Student's t-test to show if the methods provide significant differences.

### 3.1. Symmetry and transitivity error

Registration algorithms do not lead necessarily to symmetric deformation fields between reference and object images.[16] Figure 1 illustrates deformation evaluation between a set of three acquisitions (A, B, C) of a same patient for each method. Each image is alternatively reference and deformed image. Let $U_{XZ}$ denotes the deformation field estimated between X (reference) and Z (deformed), with X,Z $\in$ {A,B,C}. We evaluate the symmetry of the computed deformation field by computing the mean ($\sigma_{sym}$) and the standard deviation ($\mu_{sym}$) of $U'_{XYX}$ , with $U'_{XYX} = U_{XY} \circ U_{YX}$, which ideally is the zero vector field.

Pennec[17] proposed to perform a first evaluation of the vector field by evaluating its transitivity. Deformation field from X to Z can be written by transitivity $U'_{XYZ} = U_{XY} \circ U_{YZ}$, with Y the third image. We computed the mean ($\sigma_{tr}$) and the standard deviation ($\mu_{tr}$) of the norm of the difference between $U'_{XYZ}$ and $U_{XZ}$.

For symmetry and transitivity evaluation we only considered points belonging to the lung (lung volume and lung surface points are extracted by thresholding and morphological operations[5]).

#### 3.1.1. Jacobian and volume dilatation

We considered here operators which are related to volume variation in order to compare with lung volume computed by segmentation.

Jacobian of the deformation function measures the evolution of voxel $\boldsymbol{x}$[18] : $J_{XY}(x) = Jac(Id + U^p_{XY}(\boldsymbol{x})) = V_1(\boldsymbol{x})/V_0(\boldsymbol{x})$. $J > 1$ corresponds to a local dilatation, $J < 1$ to a local contraction and $J = 1$ to no volume change. We have used this operator to evaluate the coherence of the transformation: negative value of the Jacobean means that the deformation is locally non-invertible.

Divergence of the deformation function was proposed by Thirion and Calmon[19]: $div(Id + U^p_{XY})$. Divergence measures the difference between inflow and outflow through an elementary volume element. Negative divergence value means local contraction while positive value means local dilatation. Divergence is computed with 3D

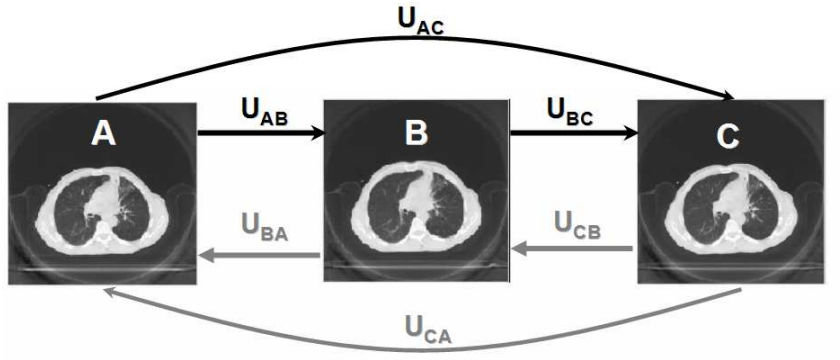


**Figure 1.** Deformation field computation scheme : each acquisition (A, B and C) is alternatively reference and object image.

Gaussian recursive filter. Each image voxel may be viewed as an elementary volume element. To differentiate contraction from dilatation, we calculated the change of volume per unit volume of each voxel according to divergence value : $\text{abs}(V_1(\boldsymbol{x}) - V_0(\boldsymbol{x}))/V_0(\boldsymbol{x})$, with $V_0(\boldsymbol{x})$ the initial volume of $\boldsymbol{x}$ and $V_1(\boldsymbol{x})$ volume after deformation. $V_1(\boldsymbol{x})$ is computed as follows. The deformation tensor for each point $\nabla U^p_{XY}(\boldsymbol{x})$ can be decomposed in a symmetric part, denoted by $V_{XY}(\boldsymbol{x})$ (local pure deformation) and an asymmetric part, denoted by $W_{XY}(\boldsymbol{x})$ (local rotation). We can write $\nabla U^p_{XY}(\boldsymbol{x}) = V_{XY}(\boldsymbol{x}) + W_{XY}(\boldsymbol{x})$, with $V_{XY}(\boldsymbol{x}) = \frac{1}{2}(\nabla U^p_{XY}(\boldsymbol{x}) + (\nabla U^p_{XY}(\boldsymbol{x}))^T)$ and $W_{XY}(\boldsymbol{x}) = \frac{1}{2}(\nabla U^p_{XY}(\boldsymbol{x}) - (\nabla U^p_{XY}(\boldsymbol{x}))^T)$. The local volume change is thus $V_1(\boldsymbol{x}) = det(V_{XY}(\boldsymbol{x}))$. Total variation of lung volume ($Vol_{XY}$) between 2 acquisitions X,Y due to residual motion is computed with equation 8.

$$Vol_{XY} = \frac{1}{N} \sum_{\boldsymbol{x} \in \Omega_X} \text{sgn}(div(Id + U^p_{XY}(\boldsymbol{x}))) \frac{\text{abs}(V_1(\boldsymbol{x}) - V_0(\boldsymbol{x}))}{V_0(\boldsymbol{x})} \tag{8}$$

$$\text{with} \quad \text{sgn}(div(Id + U^p_{XY}(\boldsymbol{x}))) = \begin{cases} 1, & \text{if } div(Id + U^p_{XY}(\boldsymbol{x})) \geq 0 \\ -1, & \text{if } div(Id + U^p_{XY}(\boldsymbol{x})) < 0 \end{cases}$$

## 4. EXPERIMENTS

### 4.1. Materials

We used clinical data sets of two patients : one with normal lung behavior and the second with bad BH reproducibility due to atelectasis and emphysema. For each, 3D CT scans are acquired in BH at a determined level of the breathing cycle (about 70% of the vital capacity). The scans have $5\,mm$ inter-plane and $0.9\,mm$ intra-plane resolution, leading to $512 \times 512 \times 65$ image resolution. Voxel values are encoded on 16 bits. As mentioned in our previous work it is important to keep the full range of Hounsfield units* related to density information.

### 4.2. Non-rigid registration parameters

Vector fields were estimated at a resolution of $256 \times 256 \times 65$ which corresponds to $1.9\,mm$ in intra-plane and $5\,mm$ inter-plane resolution. For each patient we have performed 18 non-rigid registrations (each of the 3 acquisitions is alternatively the reference and the floating image, 3 methods) leading to 36 deformation fields. For the three methods we used $\alpha \in [0.5, 0.65]$ which is equivalent to a maximum estimated vector displacement of $[0.77, 1]$ voxel by iteration. The Gaussian variance was 1.0 for the Gaussian regularization. For $M_2$ and $M_3$ a good empirical convergence was obtained with $\kappa = 0.1$ (smaller values leaded to slower convergence and values larger than 0.3 leaded to divergence). Trade-off parameter $\beta$ was set empirically to 0.5. $\xi$ was set to 0.6 (close to 1 values of

*Hounsfield density values for human body are approximatively from -1000 to 4000. 0 corresponds to water and -1000 to air.

$\xi$ lead to a Gaussian like regularization). For each registration procedure using $M_3$ we fixed $\gamma$ parameter in order to have a 70% isotropic and 30% anisotropic inside lungs behavior of the Nagel-Enckelmann regularization. Convergence for the algorithm was obtained empirically with 150 iterations for $M_1$ and at least 800 iterations for both $M_2$ and $M_3$.

## 4.3. Results

### 4.3.1. Algorithm convergence

Figure 2 illustrates the convergence of the three methods for one patient according to the iteration. The convergence criterion is the mean of absolute intensity differences between reference and deformed images.

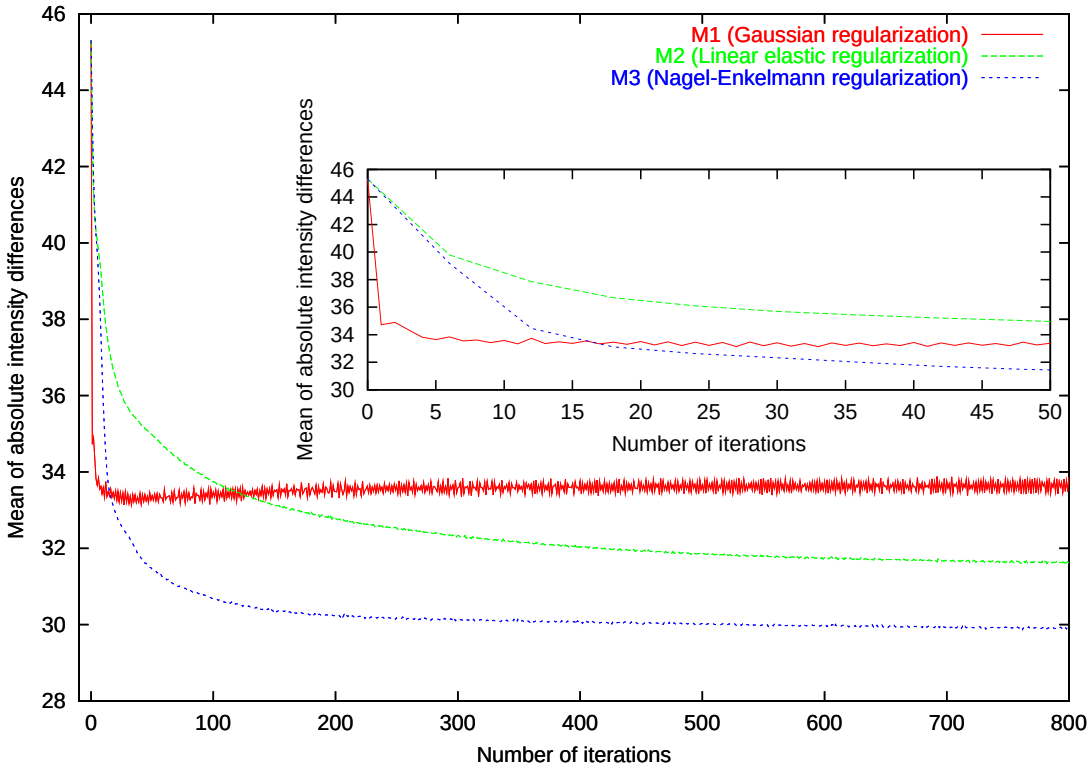


**Figure 2.** Mean of absolute intensity differences between two images with the three registration methods according to the iteration.

### 4.3.2. Displacement vectors

Table 1 presents average and standard deviation of residual motion (for lung volume points - first row and surface lung points - second row) computed on 6 vector fields by patient for each method. Figure 3 depicts a closeup region of transversal slice with projected vector field computed with Gaussian regularization (a), Linear elastic regularization (b), Nagel-Enckelmann based regularization (c). It can be noticed the smoothness difference between vector field computed with $M_3$ and those computed with $M_1$ and $M_2$.

### 4.3.3. Symmetry and transitivity error

Table 2 shows the symmetry error ($\mu_{sym}$ and $\sigma_{sym}$) and table 3 the transitivity error ($\mu_{tr}$ and $\sigma_{tr}$) of the computed vector fields with $M_1$, $M_2$ and $M_3$ for the two patients. Values are given in mm.

**Table 1.** Mean and standard deviation (in mm) of vector displacements for the 3 methods and 2 patients for lung volume points and lung surface points.

| Displacement vectors | Patient 1 | | | Patient 2 | | |
|---|---|---|---|---|---|---|
| | $M_1$ - $\mu_d(\sigma_d)$ | $M_2$ - $\mu_d(\sigma_d)$ | $M_3$ - $\mu_d(\sigma_d)$ | $M_1$ - $\mu_d(\sigma_d)$ | $M_2$ - $\mu_d(\sigma_d)$ | $M_3$ - $\mu_d(\sigma_d)$ |
| Lung volume | 3.35 (2.00) | 2.94 (1.95) | 2.99 (2.26) | 4.32 (3.28) | 3.83 (2.77) | 4.32 (4.02) |
| Lung surface | 3.21 (2.07) | 2.92 (1.96) | 2.78 (2.25) | 3.96 (3.18) | 3.48 (2.71) | 3.71 (3.64) |

**Figure 3.** Closeup region of transversal slice with projected vector field computed with (a) Gaussian regularization, (b) Linear elastic regularization, (c) Nagel-Enckelmann based regularization. The vector field was downsampled to 2mm for a better visualization.

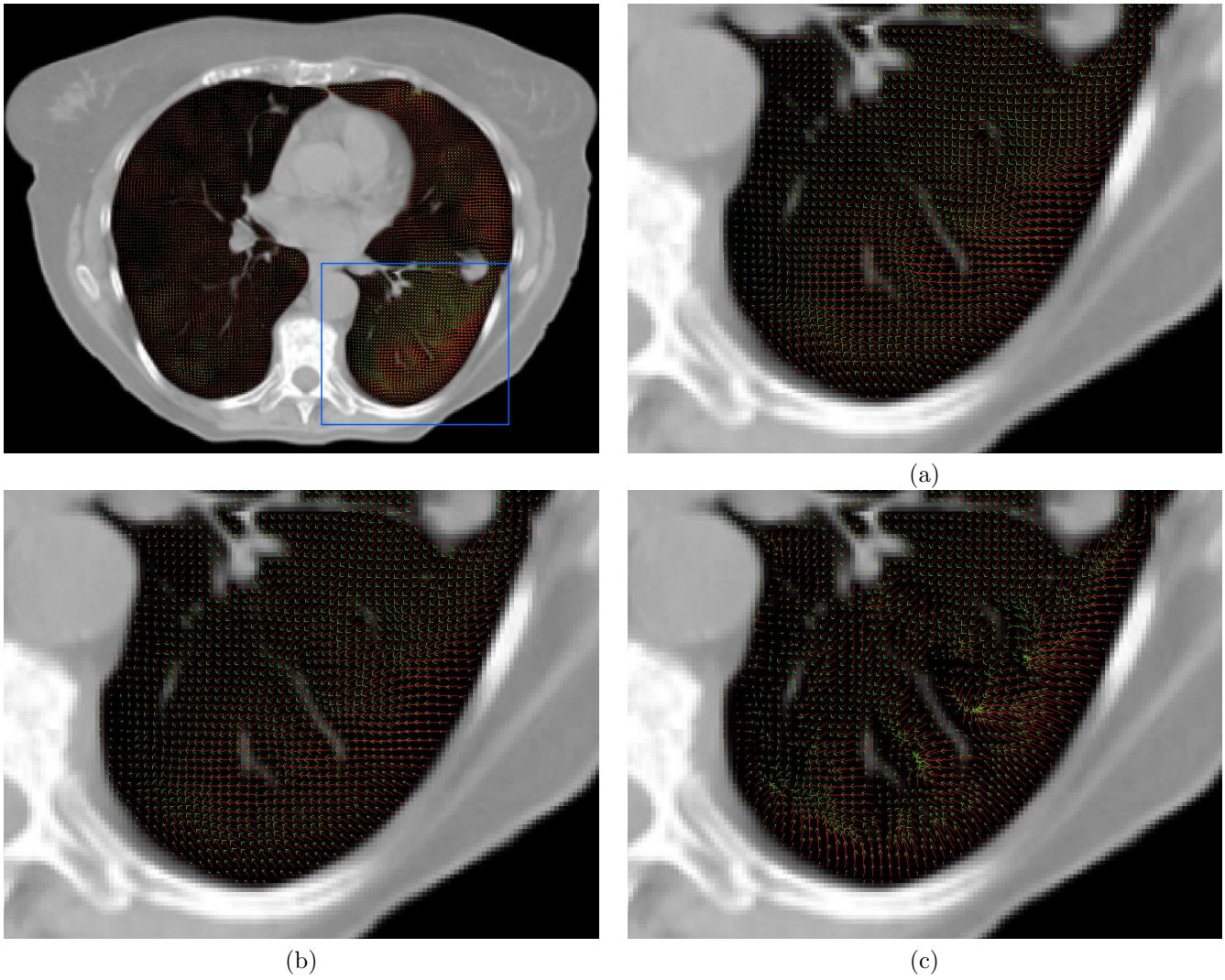

(a)

(b)

(c)

#### 4.3.4. Jacobian and volume dilatation

Left table 4 shows the percentage of points with negative Jacobian for the two patients and the three methods. For each method, last rows shows for each patient the mean percentage of negative Jacobian points of the six vector fields.

Right table 4 shows the percentage of lung volume change between acquisitions computed from lung masks

(first column) and computed with previously described local dilatation operators (2 other columns). Positive values correspond to volume increases and negative values to volume decreases. For each patient, last row shows for each method the mean of absolute differences ($\text{Dil}_{err}$) between the volume change computed with dilatation operator and volume change computed by segmentation.

**Table 2.** Mean and standard deviation error (in mm) of the deformation for the 3 methods and 2 patients according to the symmetry property.

| | $M_1$ | | $M_2$ | | $M_3$ | |
|---|---|---|---|---|---|---|
| Deformation symmetry | Patient 1 $\mu_{sym}(\sigma_{sym})$ | Patient 2 $\mu_{sym}(\sigma_{sym})$ | Patient 1 $\mu_{sym}(\sigma_{sym})$ | Patient 2 $\mu_{sym}(\sigma_{sym})$ | Patient 1 $\mu_{sym}(\sigma_{sym})$ | Patient 2 $\mu_{sym}(\sigma_{sym})$ |
| $U'_{ABA}$ | 0.8 (0.5) | 2.3 (3.9) | 0.7 (0.5) | 1.6 (2.4) | 1.3 (1.1) | 2.0 (2.2) |
| $U'_{BAB}$ | 1.0 (0.7) | 2.2 (3.3) | 0.6 (0.5) | 1.6 (2.0) | 1.3 (1.1) | 2.2 (2.1) |
| $U'_{ACA}$ | 1.2 (0.9) | 1.2 (1.8) | 1.1 (0.8) | 0.9 (1.1) | 2.1 (1.4) | 1.4 (1.4) |
| $U'_{CAC}$ | 1.2 (0.9) | 1.2 (1.7) | 1.1 (0.8) | 1.0 (1.1) | 2.2 (1.6) | 1.5 (1.6) |
| $U'_{BCB}$ | 0.8 (0.6) | 2.0 (3.2) | 0.7 (0.5) | 1.4 (2.0) | 1.4 (1.5) | 1.9 (2.0) |
| $U'_{CBC}$ | 0.9 (0.7) | 2.6 (3.9) | 0.6 (0.4) | 1.9 (2.4) | 1.2 (1.1) | 2.4 (2.5) |
| Mean | 1.0 (0.7) | 1.9 (3.0) | 0.8 (0.6) | 1.4 (1.8) | 1.6 (1.3) | 1.9 (2.0) |

**Table 3.** Mean and standard deviation error (in mm) of the deformation for the 3 methods and 2 patients according to the transitivity property.

| | $M_1$ | | $M_2$ | | $M_3$ | |
|---|---|---|---|---|---|---|
| Deformation transitivity | Patient 1 $\mu_{tr}(\sigma_{tr})$ | Patient 2 $\mu_{tr}(\sigma_{tr})$ | Patient 1 $\mu_{tr}(\sigma_{tr})$ | Patient 2 $\mu_{tr}(\sigma_{tr})$ | Patient 1 $\mu_{tr}(\sigma_{tr})$ | Patient 2 $\mu_{tr}(\sigma_{tr})$ |
| $U'_{ACB}$ | 1.6 (0.9) | 2.5 (2.3) | 1.8 (1.1) | 2.1 (1.9) | 2.4 (1.5) | 2.8 (3.0) |
| $U'_{BCA}$ | 1.7 (1.0) | 2.5 (2.5) | 1.5 (0.8) | 2.0 (1.9) | 1.9 (1.2) | 2.5 (2.7) |
| $U'_{ABC}$ | 1.5 (0.9) | 2.8 (3.4) | 1.8 (1.1) | 2.1 (1.9) | 2.3 (1.4) | 3.4 (4.7) |
| $U'_{CBA}$ | 1.5 (0.8) | 3.5 (4.7) | 3.9 (2.6) | 4.3 (2.3) | 3.7 (2.8) | 4.8 (4.1) |
| $U'_{BAC}$ | 1.5 (0.9) | 2.5 (2.5) | 1.9 (1.1) | 2.1 (1.9) | 2.6 (1.5) | 2.5 (2.7) |
| $U'_{CAB}$ | 1.6 (0.9) | 2.6 (2.6) | 1.5 (0.8) | 2.1 (1.9) | 1.9 (1.4) | 2.8 (3.1) |
| Mean | 1.6 (0.9) | 2.7 (3.0) | 2.1 (1.3) | 2.5 (2.0) | 2.5 (1.6) | 3.1 (3.4) |

**Table 4.** (Left table) Percentage of points with negative Jacobian computed on each vector field for the 3 methods and the 2 patients. (Right table) Lung volume dilatation for 3 images comparisons for 2 patients. Each column depicts the volume change (in %, computed from segmented lung) and the dilatation operator computed with the resulting vector field of the 3 methods.

| Jacob. | $M_1$ | | $M_2$ | | $M_3$ | |
|---|---|---|---|---|---|---|
| | P1(%) | P2(%) | P1(%) | P2(%) | P1(%) | P2(%) |
| $J_{AB}$ | 1.3 | 10.1 | 0.6 | 6.5 | 4.5 | 18.3 |
| $J_{BA}$ | 6.2 | 6.2 | 4.0 | 3.3 | 12.1 | 9.8 |
| $J_{AC}$ | 2.1 | 5.5 | 0.7 | 2.7 | 7.5 | 9.2 |
| $J_{CA}$ | 5.7 | 9.2 | 3.0 | 5.9 | 14.0 | 15.1 |
| $J_{BC}$ | 3.4 | 5.6 | 1.7 | 2.6 | 6.8 | 9.5 |
| $J_{CB}$ | 1.4 | 16.7 | 0.6 | 12.1 | 4.7 | 24.1 |
| Mean | 3.4 | 8.9 | 1.8 | 5.5 | 8.3 | 14.3 |

| Dilat. | Patient 1 (%) | | | | Patient 2 (%) | | | |
|---|---|---|---|---|---|---|---|---|
| | $V_{seg}$ | $M_1$ | $M_2$ | $M_3$ | $V_{seg}$ | $M_1$ | $M_2$ | $M_3$ |
| $Vol_{AB}$ | 3.9 | 3.3 | 2.8 | 3.4 | -6.6 | -6.5 | -6.0 | -7.1 |
| $Vol_{BA}$ | -3.9 | -4.5 | -3.7 | -4.5 | 6.6 | 4.8 | 4.4 | 5.6 |
| $Vol_{AC}$ | 4.1 | 3.6 | 3.3 | 3.7 | 5.6 | 4.4 | 4.1 | 4.8 |
| $Vol_{CA}$ | -4.1 | -5.0 | -4.6 | -5.3 | -5.6 | -6.2 | -5.8 | -6.4 |
| $Vol_{BC}$ | 0.4 | -1.2 | -1.0 | -0.8 | 13.1 | 10.5 | 9.5 | 12.8 |
| $Vol_{CB}$ | -0.4 | -0.3 | -0.4 | -0.7 | -13.1 | -12.2 | -11.0 | -13.0 |
| $\text{Dil}_{err}$ | - | 0.7 | 0.7 | 0.7 | - | 1.2 | 1.7 | 0.6 |

#### 4.3.5. Statistical methods comparisons

Table 5 depicts Student's t-test between the three methods for each vector field operator. "=" denotes that two methods are not significantly different. If two methods are different, "+" denotes a 95% level for p=0.05 (significant different), "++" denotes a 99% level for p=0.01 (highly significant different) and "+++" denotes a 99.9% level for p=0.001 (very highly significant different).

**Table 5.** Table depicts Student's t-test between the three methods for each vector field operator."=" denotes not significantly different,"+" significantly different, "++" highly significantly different and "+++" very highly significantly different.

| Operator | $M_1/M_2$ | $M_1/M_3$ | $M_2/M_3$ |
|---|---|---|---|
| Symmetry error | = | = | ++ |
| Transitivity error | = | + | = |
| Jacobian | = | + | +++ |
| Dilatation | = | = | = |

## 5. DISCUSSION

Gaussian regularization leads to faster convergence (about 150 iterations) than linear elastic and Nagel-Enckelmann based regularizations which require a minimum of 800 iterations for patient 1 and even more iterations for patient 2 (with larger deformations).

We noticed that the symmetry and transitivity errors for each method are relatively larger for patient 2 compared to patient 1. $M_3$ leads to larger symmetry error than $M_2$ (at 99% level for p=0.01) and larger transitivity error compare to $M_1$ (at 95% level for p=0.05).

The number of points with negative Jacobian can be a measure of the transformation validity. Deformation fields computed with $M_3$ present a larger number of negative Jacobian points than two others methods (at 95% level for p=0.05 compared to $M_1$ and at 99.9% level for p=0.01 compared to $M_2$). We also noticed that a global lung contraction implies a larger percentage of points with negative Jacobian.

Right table 4 compares a global measure of lung volume difference computed from segmentation with local lung volume changes computed from the vector fields in order to detect incoherent situations. We first notice that the two analysis are very close : it suggests that the computed vector fields are coherent according to the observed volume change. Moreover, the three methods are equivalent. Results are also related with the average displacements of the two patients : patient 1 presents smaller displacements than patient 2. For $Vol_{BC}$ of patient 1, we observed a lung volume dilatation when computed with segmentation although a lung volume contraction is computed with dilatation operator. It may be due to a difficult lung segmentation and to the final oscillations of the algorithms when approaching matching solution: the estimated field may be locally greater than the real deformation needed for perfect matching and thus object image is deformed more than needed. This phenomena was also observed by.[20] In the future, this information may be considered for evaluating the stop criterion of the registration algorithm.

## 6. CONCLUSION

Breath holding requires the knowledge of residual motion between two breath-holds. Non-rigid registration allows to estimate such residual motion and vector field information will be used for dose margins delivery studies. In this work, we studied three non-rigid registration schemes (Gaussian, linear elastic and Nagel-Enckelmann based regularizations) and analyzed several operators (transitivity, symmetry, dilatation, Jacobian) to compare resulting vector fields. Data sets from two patients with normal and impaired lung behavior were used. None of operators allows to clearly highlight the superiority of a method, except for convergence rapidity ($M_1$ faster) and Jacobian ($M_1$ worse). Christensen and Johnson[21] jointly estimate forward and reverse transformation between images while constraining these transformations to be inverses of one other. We plan to follow a similar scheme by estimating the deformation field using the 3 acquisitions and constraining the transformation to be transitive.

None of the analysis operators used here considers anatomical structures informations, only evaluate vector fields. Future works will exploit vector field properties together with local anatomical structure correspondences.

**Acknowledgment** : This work was supported in part by Elekta Oncology Systems.

## REFERENCES

1. M. Goitein, "Organ and Tumor Motion: An Overview," *Semin. Radiat. Oncol.* **14**, pp. 2–9, Jan. 2004.
2. "ICRU Report 62: Prescribing, Recording, and Reporting Photon Beam Therapy (Supplement to ICRU report 50). International Commission on Radiation Units and Measurements." International Commission on Radiation Units and Measurements, Bethesda, MD, 1999.
3. C. Ozhasoglu and M. Murphy, "Issues in Respiratory Motion Compensation During External-beam Radiotherapy," *International Journal of Radiation Oncology Biology Physics* **52**(5), pp. 1389–99, 2002.
4. J. Wong, M. Sharpe, D. Jaffray, V. Kini, J. Robertson, J. Stromberg, and A. Martinez, "The Use of Active Breathing Control (ABC) to Reduce Margin for Breathing Motion," *Int. J. Radiat. Oncol. Biol. Phys.* **44**, pp. 911–919, July 1999.
5. V. Boldea, D. Sarrut, and S. Clippe, "Lung Deformation Estimation with Non-rigid Registration for Radiotherapy Treatment," in *MICCAI'2003*, **2878**, pp. 770–777, LNCS, (Montreal (Canada)), 2003.
6. J. Thirion, "Image Matching as a Diffusion Process: an Analogy with Maxwell's Demons," *Medical Image Analysis* **2**(3), pp. 243–260, 1998.
7. L. Fan, C. Chen, J. Reinhardt, and E. Hoffman, "Evaluation and Application of 3D Lung Warping and Registration Model Using HRCT Images," in *Proc. SPIE Conf. Medical Imaging*, **4321**, pp. 234–243, (San Diego, Ca), 17-22 Feb. 2001.
8. L. Weruaga, J. Morales, L. Nunez, and R. Verdu, "Estimating Volumetric Motion in Thorax with Parametric Matching Constraints," *IEEE T. Med. Im.* **22**, pp. 766–772, June 2003.
9. P. Cachier, X. Pennec, and N. Ayache, "Fast Non-rigid Matching by Gradient Descent: Study and Improvements of the "Demons" Algorithm," Tech. Rep. RR3706, INRIA, 1999.
10. P. Ciarlet, *Mathematical Elasticity*, vol. 1, North Holland, Amsterdam, 1988.
11. G. Hermosillo, *Variational Methods for Multimodal Image Matching.* PhD thesis, Université de Nice Sophia-Antipolis, May 2002.
12. H.-H. Nagel and W. Enkelmann, "An investigation of smoothness constraints for the estimation of displacement vector fields from images sequences," *IEEE Trans. Pattern. Annal. Mach. Intell.* **8**, pp. 565–593, 1986.
13. M. Bro-Nielsen, *Medical Image Registration and Surgery Simulation.* PhD thesis, Technical University of Denmark, 1996.
14. P. Cachier and N. Ayache, "Regularization Methods in Non-rigid Registration: II. Isotropic Energies, Filters and Splines," Tech. Rep. 4243, INRIA, 2001.
15. F. Maes, A. Collignon, D. Vandermeulen, G. Marchal, and P. Suetens, "Multimodality Image Registration by Maximization of Mutual Information," *IEEE T. Med. Im.* **16**(2), pp. 187–198, 1997.
16. P. Rogelj and S. Kovačič, "Symmetric Image Registration," in *Proc. SPIE Conf. Medical Imaging*, **5032**, pp. 334–343, (San Diego, CA), 15-20 Feb. 2003.
17. X. Pennec, C. Guttmann, and J.-P. Thirion, "Feature-based Registration of Medical Images: Estimation and Validation of the Pose Accuracy," in *MICCAI'1998*, *LNCS* **1496**, pp. 1107–1114, Springer Verlag, (Cambridge (USA)), Oct. 1998.
18. D. Rey, G. Subsol, H. Delingette, and N. Ayache, "Automatic Detection and Segmentation of Evolving Processes in 3D Medical Images: Application to Multiple Sclerosis," *Medical Image Analysis* **6**, pp. 163–179, June 2002.
19. J.-P. Thirion and G. Calmon, "Measuring Lesion Growth from 3D Medical Images," in *Non Rigid and Articulated Motion Workshop (NAM '97) in Conjunction with CVPR '97*, June 1997.

20. H.Helminen, J.Alakuijala, K. Pesola, and J.Laitinen, "Comparision of Local External Force Functions for Non-rigid Registration of 3D Medical Images," in *MICCAI'2003*, **2879**, pp. 821–828, LNCS, (Montreal (Canada)), 2003.
21. G. Christensen and H. Johnson, "Consistant image registration," *IEEE T. Med. Im.* **20**(7), pp. 568–582, 2001.